Space-based measurements of HCl: Intercomparison and historical context

D. J. Lary[1,2] and O. Aulov[1,2]

[1]   The peak in stratospheric HCl was reached in the late 1990s. Between 1998 and 2004 the stratospheric loading of HCl was relatively constant, with some month to month fluctuation; this was followed by a more pronounced decrease in HCl since 2004. We use probability distribution functions (PDFs) and scatter diagrams for validation and bias characterization of Aura Microwave Limb Sounder (MLS) HCl retrievals. Both these methods allow us to use large statistical samples and do not require correlative measurements to be colocated in space and time. The bias between the Halogen Occultation Experiment (HALOE) and Aura MLS is greatest above the 525 K ($\sim$21 km) isentropic surface. The global average mean bias between Aura and the Atmospheric Chemistry Experiment (ACE) for January 2005 was 2% and between Aura MLS and HALOE was 14%. The widths of the PDFs are a measure of the spatial variability and measurement precision. The Aura MLS HCl PDFs are consistently wider than those for ACE and HALOE, this reflects the retrieval uncertainties. The median observation uncertainty for Aura MLS v1.51 HCl is 12%, and the median ACE v2.2 uncertainty is 8%. We also connect Aura MLS HCl with the heritage of HALOE HCl by using neural networks to learn the interinstrument biases and provide a seamless HCl record from the launch of the Upper Atmosphere Research Satellite (UARS) in 1991 to the present.

1.   Introduction

[2]   The Microwave Limb Sounder (MLS) on Aura is providing the first daily global observations of HCl [*Waters et al.*, 2006; *Froidevaux et al.*, 2006b]. A preliminary validation of MLS HCl has been presented by *Froidevaux et al.* [2006a].

[3]   Evaluation and validation of satellite data are necessary, but sampling issues can make practical application problematic. In the traditional approach to validation, there is a comparison of matched pairs of profiles coincident in space and time. This strong constraint dramatically reduces the statistical sample sizes we can deal with. The definition of "coincident" observations varies, but 1000 km or more often separates such measurements. Establishing instrument accuracy or precision through such comparisons can be hindered by the limited number of coincident pairs and the contribution of atmospheric variability (termed representativeness). Issues of representativeness arise because the validation exercises are typically limited geographically. It is therefore useful to augment the traditional approach to validation with the use of probability distribution functions (PDFs) of trace gases over an extended period for a given spatial domain. In this study, we choose to form PDFs of an entire month of data and to specify the spatial domain in terms of Lagrangian flow-tracking coordinates. The width of the PDFs allow us to quantify the spatial variability for each analysis grid cell over the month. The analysis starts with the launch of UARS and continues up to the present. The scatter diagrams allow us to compare a pair of instruments globally over the entire period of overlap using the PDFs for each month, for each Lagrangian region.

[4]   PDFs have already been used in a variety of tracer studies [*Pierrehumbert*, 1994; *Yang*, 1995; *Sparling and Schoeberl*, 1995; *Rood et al.*, 2000; *Hu and Pierrehumbert*, 2001; *Gao et al.*, 2002; *Johnson et al.*, 2002; *Strahan*, 2002; *Neu et al.*, 2003; *Hsu et al.*, 2004] and in estimation of representativeness uncertainty in chemical data assimilation [*Lary*, 2003].

[5]   Not only does a PDF characterize the tracer distribution, its shape tells us about mixing barriers, how complete the mixing is, and chemical processes such as ozone depletion [*Sparling*, 2000; *Pierrehumbert*, 2000; *Strahan*, 2002; *Neu et al.*, 2003]. For example, a narrow peak in the concentration PDF indicates that the air is well mixed and significant variability generating processes have not recently occurred (e.g., long-range transport). A multimodal distribution indicates air of different origins (e.g., polar and midlatitude). In general, broad peaks indicate recent variability-generating processes such as photochemistry or transport (horizontal or vertical).

[1] Goddard Earth Sciences and Technology Center, University of Maryland Baltimore County, Baltimore, Maryland, USA.
[2] Atmospheric Chemistry and Dynamics Branch, NASA Goddard Space Flight Center, Greenbelt, Maryland, USA.

Table 1. Instruments Used in This Study[a]

Instrument	Temporal Coverage	Reference	Median Observation Uncertainty
ACE v2.2	2004–2006	*Bernath et al.* [2005]	8%
ASUR	1993–1994, 1999, 2000	*Mees et al.* [1995]	
ATMOS v3	1992, 1993, 1994	*Zander et al.* [1992]	8%
Aura MLS v1.51	2004–2006	*Froidevaux et al.* [2006a]	12%
HALOE v19	1991–2005	*Russell et al.* [1993]	4%
MkIV	1996, 1997, 1999, 2000, 2002–2005, 2007	*Toon et al.* [1999]	10%

[a]The uncertainties given are the median uncertainty of all the level 2 product uncertainties for all the observations made by each instrument. The HALOE uncertainties are only estimates of random error and do not include any indications of overall accuracy.

[6] Measurement imprecision is one factor that affects the widths of the PDFs, and precision of the measurements is certainly a parameter that needs validation. Because a major component of the variability of trace gases is due to atmospheric transport we make our comparisons in equivalent PV latitude–potential temperature coordinates [*Schoeberl et al.*, 1989; *Proffitt et al.*, 1989; *Lait et al.*, 1990; *Douglass et al.*, 1990; *Lary et al.*, 1995; *Schoeberl et al.*, 2000]. Using these coordinates also extends the effective latitudinal coverage of the measurements, although there will always be limitations arising from sampling issues. In the period 1991–2004 we use the UKMO meteorological analyses, and after that we use NASA GEOS meteorological analyses.

[7] Section 2 describes the HCl intercomparison using PDFs and scatter diagrams and the cross calibration of HCl retrievals using neural networks. Section 3 presents a continuous time series of HCl from the launch of UARS to the present. Section 4 gives a summary.

2. HCl Intercomparison

[8] We compare measurements of HCl from the different instruments in Table 1. Table 1 also gives the median observation uncertainty over the entire record of each instrument. The Halogen Occultation Experiment (HALOE) provides the longest record of space based HCl observations. Aura MLS has a vertical resolution which is 3 km in the lower stratosphere increasing to 5–6 km near 1 hPa and 7 km near 0.22 hPa. ACE and HALOE have a vertical resolution of about 4 km. The ACE and HALOE retrievals are given on a much finer altitude grid, with a spacing of 1 km or less. The Aura MLS retrievals used are given on a pressure grid with an approximate altitude spacing of ~2.5 km.

2.1. PDFs

[9] Figure 1 shows example HCl PDFs for the three instruments HALOE, ACE and Aura MLS. In each case the PDFs are for all observations made by that instrument in a Lagrangian region for three isentropic levels centered on an equivalent latitude of 55°N during all the Januarys that the instruments observed (Figures 1a to 1c) or for the observations made only during January 2005 (Figures 1d to 1f). A consistent picture is seen in these plots: Aura MLS agrees very well with ACE, while HALOE HCl retrievals are lower than those from the other instruments. There is a general increase in the bias with increasing altitude, particularly noticeable at the 525 K (~21 km) surface and above.

Previous comparisons among HCl data sets reveal a similar bias for HALOE [*Russell et al.*, 1996; *McHugh et al.*, 2005; *Froidevaux et al.*, 2006a].

2.2. Width of the PDFs

[10] The width of the PDFs, σ_{rep}, gives us a measure of the spatial variability (representativeness) in the tracer field [*Lary*, 2003]. A robust estimator of the width of the distribution is the average deviation [*Press et al.*, 1992],

$$\sigma_{rep} = ADev(y_1 \ldots y_N) = \frac{1}{N} \sum_{j=1}^{N} |y_j - \bar{y}| \qquad (1)$$

where y is the tracer volume mixing ratio (VMR), and the overbar indicates the mean of the N observations considered. It is interesting to look at a cross section of the representativeness as it highlights the regions with large gradients. Figure 2 shows the PDF width for HCl observations made by Aura MLS during January 2005. The upwelling air over the tropics is visible as is the large spatial variability in the lower stratospheric polar vortex at high northern latitudes.

[11] The width of the PDF could be characterized in several ways. Two other common measures are the variance, or its square root, the standard deviation. Both of these measures have been tried and give essentially the same results. The reason for choosing the average deviation is that the variance and standard deviation depend on the second moment of the PDF and can be unduly affected by a few outliers. The average deviation is a more robust estimator that does not suffer from this problem [*Press et al.*, 1992].

[12] The PDF width is actually a function of several things including spatial variability, sampling, and retrieval uncertainty and noise. The all years January plots in Figures 1a–1c clearly include a wider variety of situations than do the specific January plots (Figures 1d–1f), so as would be expected, these PDFs are wider. It is interesting to note that even though the median values of the Aura MLS and ACE PDFs are very similar, the width of the Aura MLS HCl PDFs are consistently larger than those for ACE and HALOE, this may well reflect in part the retrieval uncertainties shown in Table 1. The median observation uncertainty for Aura MLS HCl is 12%, which is 50% larger than the median ACE v2.2 uncertainty of 8%. However, the instruments generally have a similar spatial distribution, e.g., both Aura MLS and ACE have wide PDFs for the lower stratosphere vortex, and narrow PDFs in the upper

January of all years

(a)   (b)   (c)

January 2005

(d)   (e)   (f)
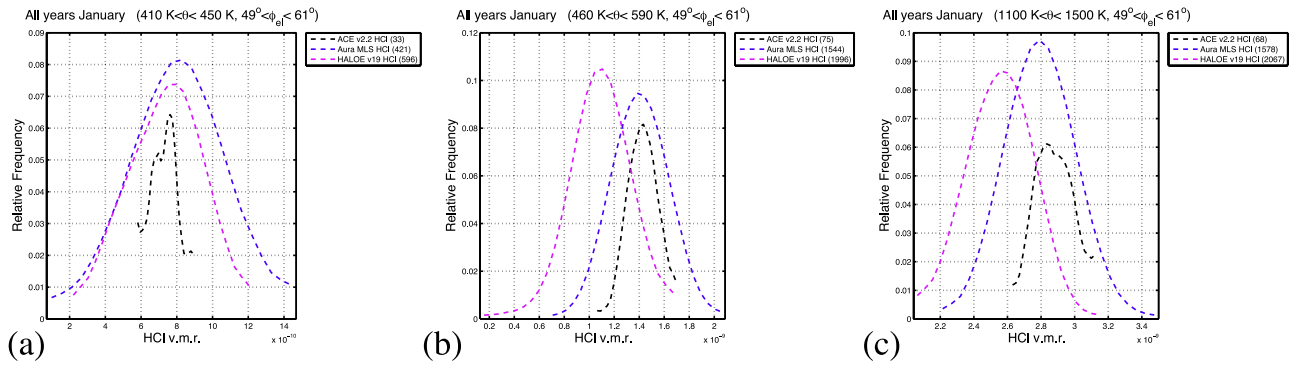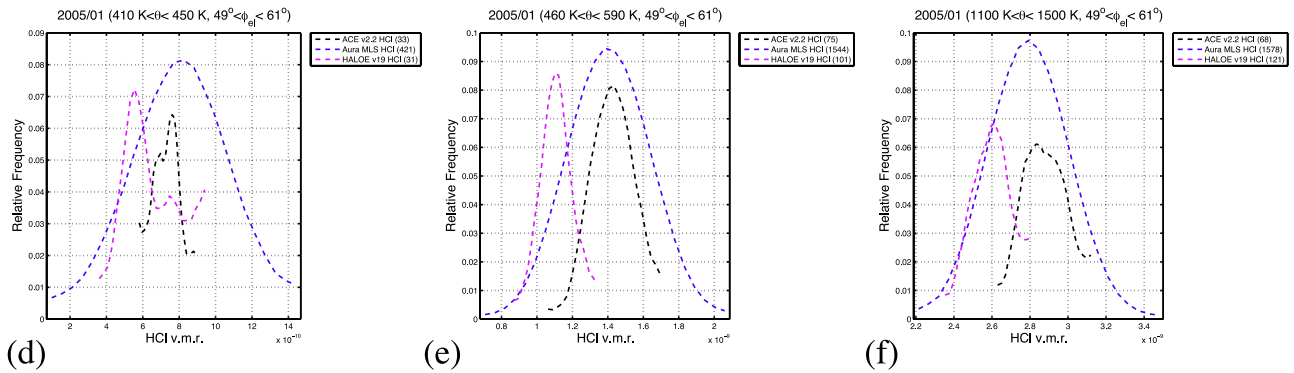
Figure 1. Example HCl PDFs for the three instruments HALOE, ACE, and Aura MLS. In each case the PDFs are for all observations made by that instrument in a Lagrangian region for three isentropic levels centered on an equivalent latitude of 55°N during all the Januarys that the instrument observed. For ACE the plots include January 2004–2006, for HALOE the plots include 2004–2005, and for MLS the plots include 2005–2006. (a) Plot of a PDF for all observations in the range 410 K < θ < 450 K (70 mbar < P < 110 mbar), 49° < ϕ_{el} < 61°. (b) Plot of a PDF for all observations in the range 460 K < θ < 590 K (30 mbar < P < 60 mbar), 49° < ϕ_{el} < 61°. (c) Plot of a PDF for all observations in the range 1100 K < θ < 1500 K (2 mbar < P < 4 mbar), 49° < ϕ_{el} < 61°. (d) to (f) Analogous to Figures 1a to 1c for the observations made only during January 2005. The number of observations used to form each PDF is shown in parentheses in the legend.
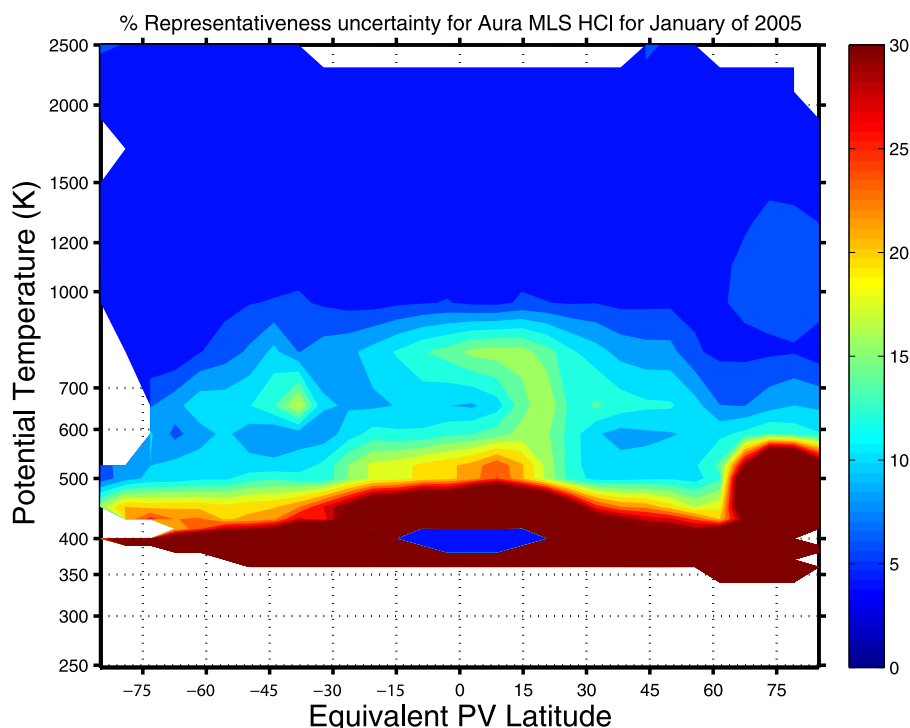
Figure 2. PDF width characterized by the average deviation for HCl observations made by Aura MLS during January 2005. The width of the PDFs, σ_{rep}, gives us a measure of the spatial variability (representativeness) in the tracer field and highlights the regions with large spatial gradients.

stratosphere. Likewise, the HALOE PDFs for a given month, are narrower than the ACE PDFs and the median HALOE uncertainty is less than median ACE observation uncertainty (e.g., Figures 1a–1c). As pointed out by E. Remsberg (personal communication, 2007), the width of the PDFs also depends on the spatial extent of the observations. For example, HALOE made sunrise measurements in the northern hemisphere from 1–9 January and from about 16 January to the end of the month. HALOE obtained data in the regions shown in Figure 1 for only a few days of January 2005. Because there is normally a lot of wave activity in the northern hemisphere in January, it would be easy for HALOE not to see a lot of the variability that was present for the month of January for that latitude zone. And that lack of coverage for the month is another reason for the narrower HALOE PDFs in Figures 1d–1f.

2.3. Biases

[13] We can take the difference between the medians of the PDFs as a measure of the interinstrument bias. This bias is really only significant if it is larger than the atmospheric variability in the Lagrangian region we are considering.

[14] Figure 3 shows interinstrument biases for January 2005 for Aura, ACE and HALOE. Figures 3a, 3c, and 3e show the bias as a volume mixing ratio (VMR). Figures 3b, 3d, and 3f show the percentage bias. Figures 3a to 3d are for the biases between ACE v2.2 and Aura MLS v01. In Figures 3a and 3b we show all available Lagrangian regions where both ACE and Aura made observations during January 2005. In Figures 3c and 3d we only plot Lagrangian regions where the bias was greater than the natural HCl variability

in that region of the atmosphere, we have called this the useful bias. The natural variability (representativeness) has been diagnosed by taking the width of the PDF as measured by the average deviation of the PDF.

[15] We note that for the January 2005 example, the bias between Aura and ACE in the lower stratosphere is less than the natural variability. The average mean bias between Aura and ACE for January 2005 was 2.3%. Figures 3e and 3f show the analogous bias for HALOE and Aura, only those Lagrangian regions where the bias was greater than the natural HCl variability have been plotted. We note that for the January 2005 example, the bias between HALOE and Aura is greater than the natural variability throughout most of the stratosphere. The average mean bias between Aura and HALOE for January 2005 was 13.9%. In general, the number of points from both of the solar occultation instruments (HALOE and ACE) is much less than the number of points from the microwave emission instrument (MLS).

2.4. Scatter Diagrams and Cross Calibration

[16] So far, we have compared the PDFs for all overlapping Lagrangian regions for a given month. However, we can use a single scatter diagram to compare all the overlaps globally for all the months observed by each pair of instruments. Such a scatter diagram has the advantage of a huge sample size, it encompasses the entire period that a pair of instruments were making contemporaneous observations. The scatter diagram is intended as a big picture summary for all contemporaneous observations made globally. Figure 4 shows two scatter diagrams for all the contemporaneous observations of HCl made globally by two pairs of instru-
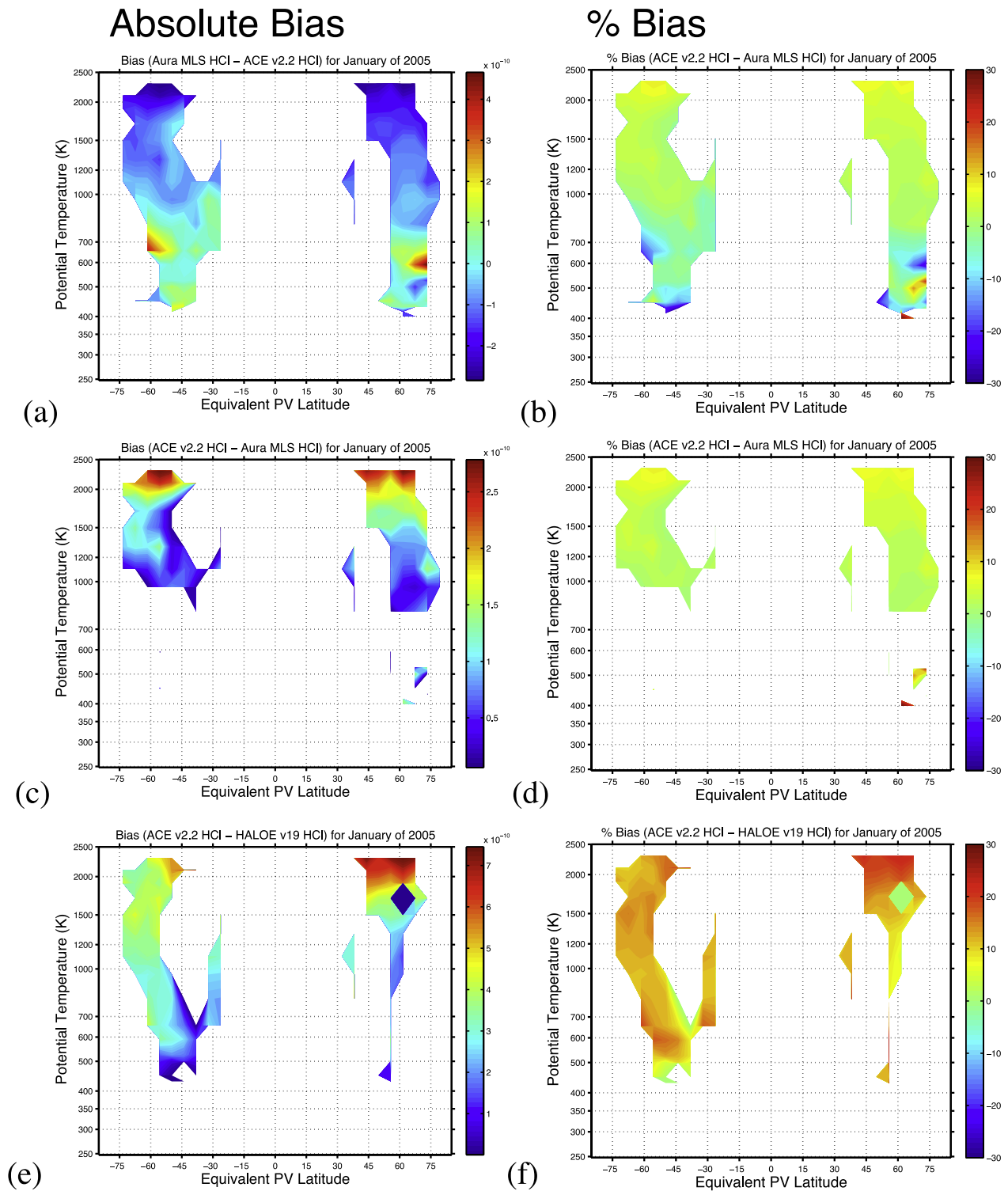
Absolute Bias   % Bias

Figure 3. Interinstrument biases for January 2005. These biases are the differences in the PDF medians for each instrument. (left) Bias as a volume mixing ratio (VMR). (right) Percentage bias. The bias is only significant if it is greater than the natural variability in that region of the atmosphere. The natural variability (representativeness) has been diagnosed by taking the width of the PDF as measured by the average deviation of the PDF. (a) to (d) For the biases between ACE v2.2 and Aura MLS v01. In Figures 3a and 3b we show all available Lagrangian regions were both ACE and Aura made observations during January 2005. In Figures 3c and 3d we only plot Lagrangian regions where the bias was greater than the natural HCl variability in that region of the atmosphere, we have called this the useful bias. It can be seen that for most of the Lagrangian regions observed by both ACE and Aura the bias is less than 10%. (e) and (f) Analogous bias for HALOE and Aura where the bias was greater than the natural HCl variability.
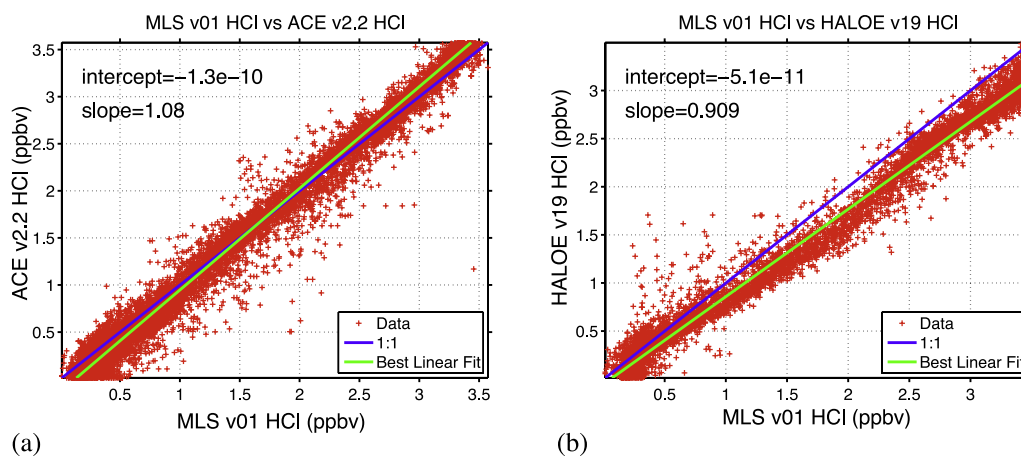
Figure 4. (a) and (b) Scatterplots of all contemporaneous observations of HCl made by HALOE, ACE, and Aura MLS. Each point plotted is the median value of a PDF of observations made for a Lagrangian region over the period of a month. It can be seen that to adequately using the slopes to describe the differences does not do justice to the differences. For example, Figure 4a shows a much better agreement than Figure 4b, but the slopes themselves do not reflect this. Figure 4b shows an offset of order 9% near 2 ppbv, whereas Figure 4a shows maybe 1 or 2% for values near 2 ppbv. The mean absolute value of the differences seems a good indicator of the fits.

ments. In Figure 4a we compare ACE and Aura MLS which were making contemporaneous observations between September 2004 and the present. In Figure 4b we compare HALOE and Aura MLS which were making contemporaneous observations between September 2004 and November 2005.

[17] In the ideal case where we have perfect agreement between two instruments, the slope of the scatter diagram would be 1 and the intercept would be 0. In the case of ACE and Aura, we see there is a slope of 1.08, and for HALOE Aura there is a slope of 0.91. It can be seen that solely using the slopes does not do justice to the differences. For example, Figure 4a shows a much better agreement than Figure 4b, but the slopes themselves do not reflect this. Figure 4b shows an offset of order 9% near 2 ppbv, whereas Figure 4a shows maybe 1 or 2% for values near 2 ppbv. The mean absolute value of the differences seems a good indicator of the fits. We also note that in the case of Aura MLS and HALOE, the scatter diagrams do not have a constant slope over the entire range of HCl values, several "wiggles" are present. This means that the interinstrument biases are spatially and temporally dependent. Neural networks are multivariate, nonparametric, "learning" algorithms that are ideally suited to learning, and correcting for, such interinstrument biases.

[18] We have used a neural network with three inputs and one output. The inputs are equivalent PV latitude, potential temperature, and HCl from instrument A. The output is HCl from instrument B. Potential temperature and equivalent latitude are used because they are good markers of the large-scale flow pattern [*Lary and Mussa*, 2004]. When we do the training we randomly split our training data set into three portions of 80%, 10% and 10%. The 80% is used to train the neural network weights. This training is iterative and on each iteration we evaluate the current RMS error of the neural network. The RMS error is calculated by using the second 10% of the data that was not used in the training. We

use the RMS error and the way it changes with training iteration (epoch) to determine the convergence of our training. When the training is complete, we use the final 10% as a validation data set. This 10% of the data was randomly chosen and not used in either the training or RMS evaluation. We only use the neural network if the validation scatter diagram, which plots the actual data from validation portion against the neural network estimate, yields a straight line graph with a slope of 1. This is a stringent and independent validation. The validation is global as the data was randomly selected over all temporal and spatial data points available. Several training strategies were examined, the one described included the most species over the longest time period. The neural network algorithm used was a feed-forward back-propagation network with 20 hidden nodes. The training was done by the Levenberg-Marquardt back-propagation algorithm provided by the Matlab neural network toolbox (available at http://www.mathworks.com/products/neuralnet/).

[19] Figures 5a and 5c show the results of such a neural network training to learn interinstrument biases between ACE v2.2, Aura MLS v1 and HALOE v19 HCl. Figures 5b and 5d show an independent validation of the training using a randomly chosen, totally independent, data sample not used in training the neural network. In each case the x axis shows the actual ACE v2.2 HCl (the target). In Figures 5a and 5b the y axis is the neural network estimate of ACE v2.2 HCl based on Aura MLS v01 HCl. Figure 5a shows the results using the training data, Figure 5b shows the results of the independent validation. In Figures 5c and 5d the y axis is the neural network estimate of ACE v2.2 HCl based on HALOE v19 HCl. Figure 5c shows the results using the training data, and Figure 5d shows the results of the independent validation. The mapping has removed the bias between the measurements and has also straightened out the "wiggles" seen in Figure 4.

Training   Independent Validation

Recalibrating Aura MLS HCl to agree with ACE v2.2 HCl

(a)

(b)

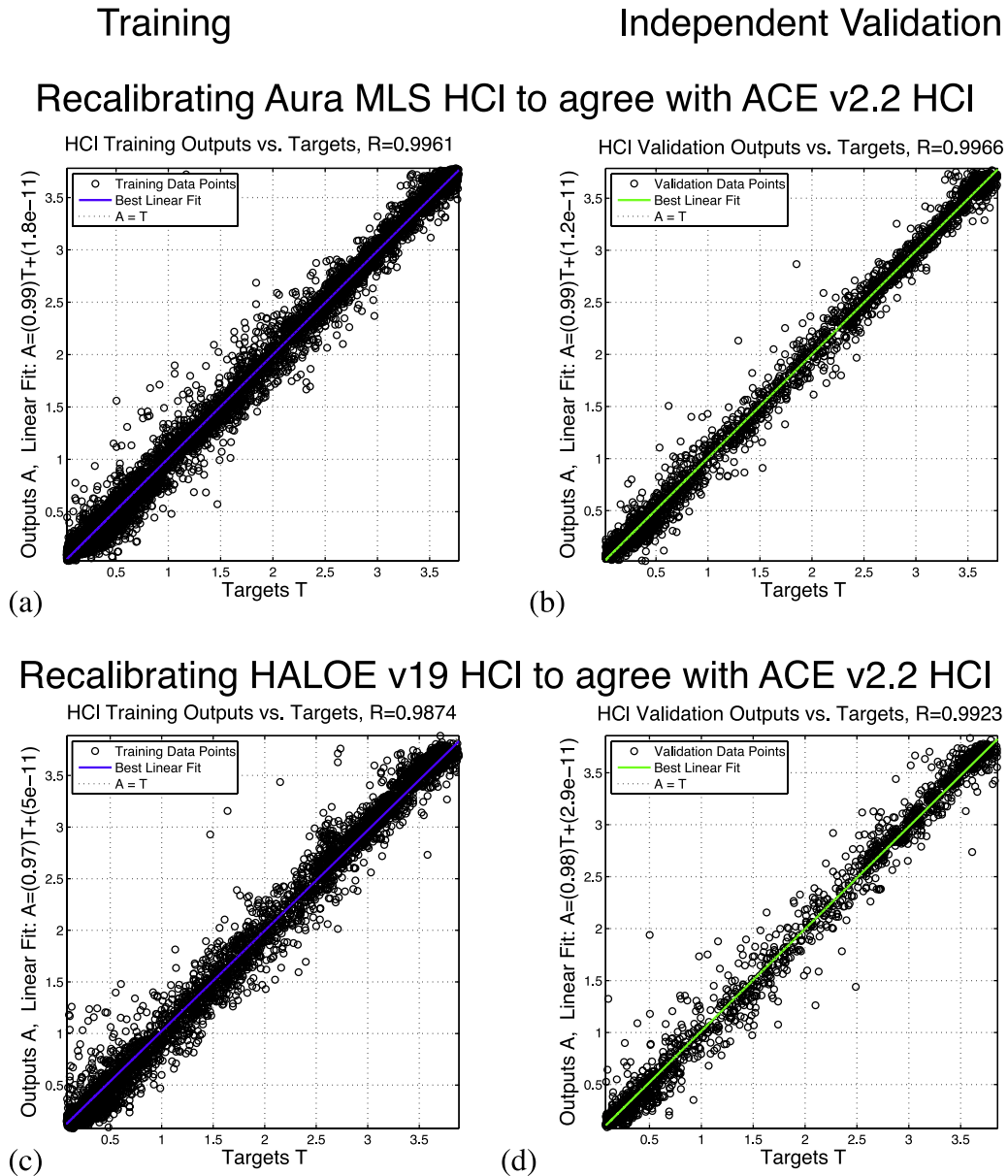### Recalibrating HALOE v19 HCl to agree with ACE v2.2 HCl

(c)

(d)

Figure 5. (left) Result of training a neural network to learn the interinstrument biases. (right) An independent validation of this training using a randomly chosen, totally independent, data sample not used in training the neural network. In each case, the x axis shows the actual ACE v2.2 HCl (the target). (a) and (b) The y axis is the neural network estimate of ACE v2.2 HCl based on Aura MLS v01 HCl. Figure 5a is the result using the training data, and Figure 5b is the result of the independent validation. (c) and (d) The y axis is the neural network estimate of ACE v2.2 HCl based on HALOE v19 HCl. Figure 5c is the result using the training data, and Figure 5d is the result of the independent validation. In each case, this is a global training for all contemporaneous observations between each pair of instruments. The training points are the median values of a PDF of observations made during a given month for a given equivalent PV latitude–potential temperature bin. The width of the cloud of points in each of these scatter diagrams is a good measure of the uncertainty associated with the neural network fit.

Table 2. Evaluating Goodness of Fit[a]

Product	χ_r^2	Number of Bins
ACE v2.2		
HALOE v19	24	5480
HALOE v19 NN calibrated as MLS	15.3	5480
HALOE v19 NN calibrated as ACE	12.7	5480
Aura MLS v1	**11.4**	8895
ATMOS		
HALOE v19	9.47	561
HALOE v19 NN calibrated as MLS	3.68	561
HALOE v19 NN calibrated as ACE	**3.51**	561
Aircraft ASUR		
HALOE v19	63.8	477
HALOE v19 NN calibrated as ACE	39.6	477
HALOE v19 NN calibrated as MLS	**36.9**	477

[a]The χ_r^2 statistics for a variety of HCl products. In order to be more critical, HCl validation products were only used if the fractional observational uncertainty for the benchmark observation was less than 0.1. For each benchmark instrument the results are sorted in descending order of χ_r^2, so the last product in each group is the product that agreed most closely with the benchmark instrument, the χ_r^2 for this instrument is shown in bold. The number of contemporaneous bins which were available for each comparison is shown.

2.5. Evaluating the Goodness of Fit

[20] We have objectively evaluated the goodness of the neural network fit by using the reduced χ_r^2 metric, which is really just the root mean square deviation normalized to measurement errors,

$$\chi_r^2 = \frac{1}{\nu} \sum_{j=1}^{N} \frac{(y_{NN} - y_j)^2}{\sigma_j^2} \qquad (2)$$

where y_{NN} is the neural network estimate of the benchmark observation, y is the benchmark observation, and σ is the observation uncertainty, $\nu = N - n$ is the degrees of freedom, N is the total number of benchmark observations, and n is the number of parameters used in the fit.

[21] Table 2 shows the reduced χ_r^2 statistics for a variety of HCl products. In order to be more critical the HCl validation products were only used if the fractional observational uncertainty of the benchmark observation was less than 0.1. For each benchmark instrument the results in Table 2 are sorted in descending order of χ_r^2, so the last product in each group is the product that agreed most closely with the benchmark instrument. In each case the product with the largest (worst) χ_r^2 was HALOE HCl, and applying a neural network recalibration considerably improved the agreement with the benchmark instruments (reduced χ_r^2).

3. HCl Time Series

[22] Now that we have completely characterized the interinstrument biases and been able to correct for them we can connect Aura MLS HCl observations to the heritage of HALOE. This allows us to produce an HCl time series from the launch of UARS in 1991 up-to the present. Figure 6 shows HCl time series for six different locations (on the 525 K ≈ 21 km, 800 K ≈ 30 km, 1300 K ≈ 41 km, and 2100 K ≈ 50 km isentropic surfaces) from the launch of

UARS to the present with HCl observations from HALOE, ATMOS, ACE, MkIV and Aura MLS.

[23] Figure 6 (left) uses the original v19 HALOE data, and the low bias of HALOE HCl relative to all other instruments is evident. Figure 6 (right) uses the HALOE v19 data recalibrated with a neural network to agree with ACE v2.2 HCl. If we compare Figures 6 (left) and 6 (right) we see that as expected, the recalibration brings the HALOE data into good agreement with ACE and Aura MLS data, and the independent ATMOS HCl data.

[24] We also performed a recalibration of the ACE and MLS data to agree with HALOE v19. These two HCl recalibrations have been used by *Lary et al.* [2007] to form a long Cl$_y$ time series and associated uncertainty estimate (typically ≤0.4 ppbv at 800 K). The uncertainty in the Cl$_y$ estimate is primarily due to the discrepancy between the different observations of HCl, i.e., the HALOE, Aura MLS, and ACE interinstrument biases.

[25] We have attempted to characterize the biases as "exactly" as possible for each space region. What we do not do, due to a lack of temporal overlap, is have the bias varying with time. Artifacts of this do appear to be evident in some of the neural network adjustments, for example, in the upper stratosphere, the adjustment of HALOE to MLS HCl seems to yield a time series which is too flat, this is true to a lesser extent for the HALOE to ACE HCl adjustment. We note that the size of the training data set plays a role, the overlap between HALOE and MLS is rather short and the result of this can be seen in Figure 6e the corrected time series using this short overlap (blue line) has the wrong shape. The the overlap between HALOE and ACE is longer and the red line in Figure 6e does not suffer from this artifact. We are currently working on trying to improve this.

4. Summary

[26] We have used PDFs to characterize the interinstrument biases between the HCl products provided by Aura MLS v01, ACE v2.2, and HALOE v19. These biases are presented in a number of ways, including global equivalent latitude potential temperature cross sections for every month of overlap between the instruments (available from http://www.pdfcentral.info/). The bias between HALOE and Aura MLS is greatest above the 525 K (~21 km) isentropic surface. The global average mean bias between Aura and ACE for January 2005 was 2% and between Aura and HALOE was 14%. A scatter diagram compares all the overlaps globally for all the months observed by a pair of instruments.

[27] The width of the PDFs are a measure of the spatial variability. The Aura MLS HCl PDFs are consistently larger than those for ACE and HALOE, this reflects the retrieval uncertainties. The median observation uncertainty for Aura MLS HCl is 12%, which is 50% larger than the median ACE v2.2 uncertainty of 8%. The instruments generally have a similar spatial distribution, e.g., both Aura MLS and ACE have wide PDFs in the lower stratosphere vortex, and narrow PDFs in the upper stratosphere.

[28] We used neural networks to correct for interinstrument biases and produce a consistent time series of HCl from 1991 to the present. Such an HCl time series is of use in estimating a time series of Cl$_y$.
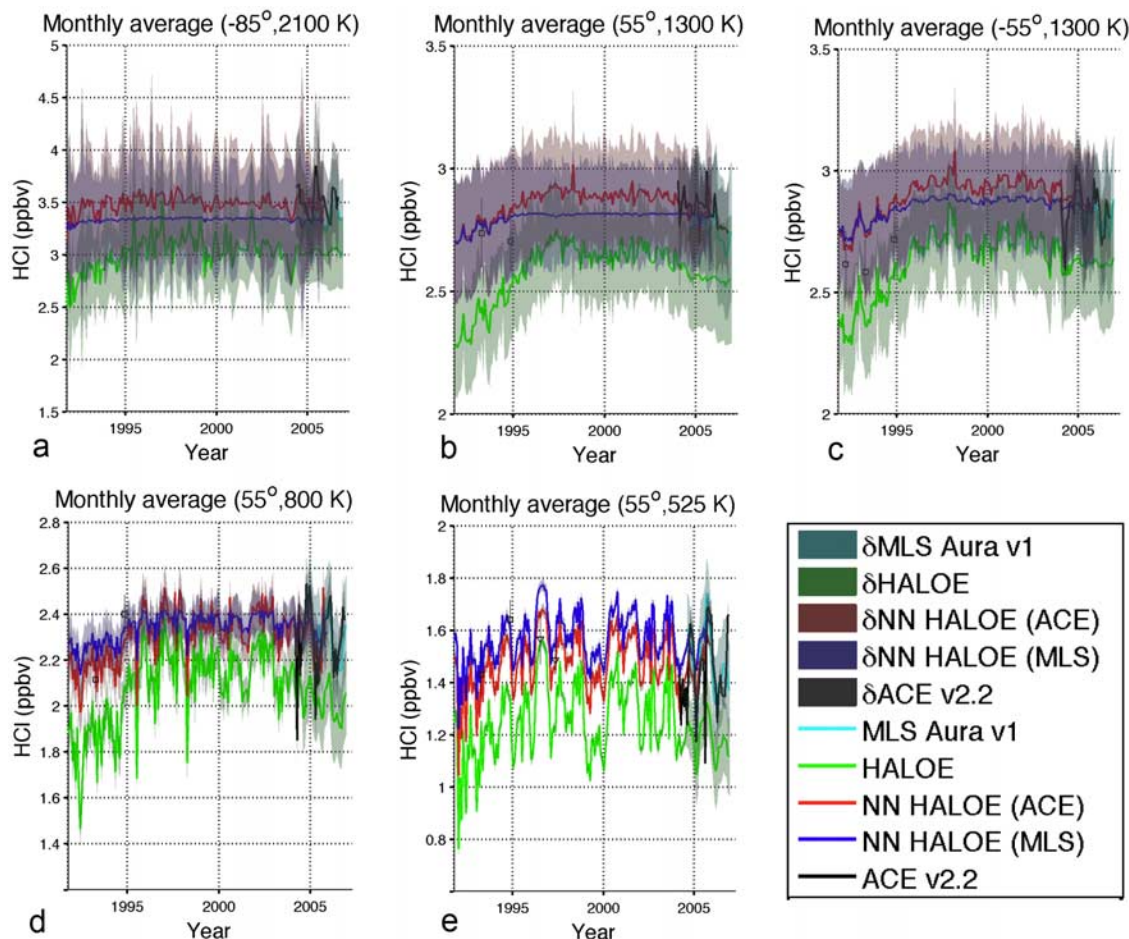
Figure 6. Selected HCl time series from the launch of UARS to the present with HCl observations from HALOE, ATMOS, ACE and Aura. (a) For 2100 K ($\sim$50 km) at 85°S, (b) and (c) for 1300 K ($\sim$41 km) at 55°N and 55°S, and (d) and (e) for 55°N at 800 K ($\sim$30 km) and 525 K ($\sim$21 km). In each case the green line and shading is for the original HALOE v19 data, and the red line and shading is for HALOE data remapped with a neural network to agree with Aura MLS v1 HCl. The black line is the ACE v2.2 data with the grey shading representing the associated uncertainty. The δ in the legend which labels the shading refers to the total uncertainty (observational, representativeness, and where relevant, neural network adjustment). The remapping of HALOE generally brings the HALOE data into better agreement with the ATMOS (squares) data as can also be seen from the χ_r^2 values shown in Table 2.

References

Bernath, P. F., et al. (2005), Atmospheric Chemistry Experiment (ACE): Mission overview, *Geophys. Res. Lett.*, *32*, L15S01, doi:10.1029/2005GL022386.

Douglass, A. R., R. B. Rood, R. S. Stolarski, M. R. Schoeberl, M. H. Proffitt, J. J. Margitan, M. Loewenstein, J. R. Podolske, and S. E. Strahan (1990), Global three-dimensional constituent fields derived from profile data, *Geophys. Res. Lett.*, *17*(4), 525–528.

Froidevaux, L., et al. (2006a), Early validation analyses of atmospheric profiles from EOS MLS on the aura satellite, *IEEE Trans. Geosci. Remote Sens.*, *44*(5), 1106–1121.

Froidevaux, L., et al. (2006b), Temporal decrease in upper atmospheric chlorine, *Geophys. Res. Lett.*, *33*, L23812, doi:10.1029/2006GL027600.

Gao, R. S., et al. (2002), Role of NO$_y$ as a diagnostic of small-scale mixing in a denitrified polar vortex, *J. Geophys. Res.*, *107*(D24), 4794, doi:10.1029/2002JD002332.

Hsu, J., M. J. Prather, O. Wild, J. K. Sundet, I. S. A. Isaksen, E. V. Browell, M. A. Avery, and G. W. Sachse (2004), Are the TRACE-P measurements representative of the western Pacific during March 2001?, *J. Geophys. Res.*, *109*, D02314, doi:10.1029/2003JD004002.

Hu, Y., and R. T. Pierrehumbert (2001), The advection-diffusion problem for stratospheric flow. part I: Concentration probability distribution function, *J. Atmos. Sol. Terr. Phys.*, *58*(12), 1493–1510.

Johnson, D. R., A. J. Lenzen, T. H. Zapotocny, and T. K. Schaack (2002), Numerical uncertainties in simulation of reversible isentropic processes and entropy conservation: part II, *J. Clim.*, *15*(14), 1777–1804.

Lait, L., et al. (1990), Reconstruction of O$_3$ and N$_2$O fields from ER-2, DC-8, and balloon observations, *Geophys. Res. Lett.*, *17*(4), 521–524.

Lary, D. (2003), Representativeness uncertainty in chemical data assimilation highlight mixing barriers, *Atmos. Sci. Lett.*, *5*(1–4), 35–41.

Lary, D. J., and H. Y. Mussa (2004), Using an extended kalman filter learning algorithm for feed-forward neural networks to describe tracer correlations, *Atmos. Chem. Phys. Disc.*, *4*, 3653–3667.

Lary, D. J., M. P. Chipperfield, J. A. Pyle, W. A. Norton, and L. P. Riishojgaard (1995), 3-dimensional tracer initialization and general diag-

nostics using equivalent PV latitude-potential-temperature coordinates, *Q. J. R. Meteorol. Soc.*, *121*(521A), 187–210.

Lary, D. J., D. W. Waugh, A. R. Douglass, R. S. Stolarski, P. A. Newman, and H. Mussa (2007), Variations in stratospheric inorganic chlorine between 1991 and 2006, *Geophys. Res. Lett.*, *34*, L21811, doi:10.1029/2007GL030053.

McHugh, M., B. Magill, K. A. Walker, C. D. Boone, P. F. Bernath, and J. M. Russell III (2005), Comparison of atmospheric retrievals from ACE and HALOE, *Geophys. Res. Lett.*, *32*, L15S10, doi:10.1029/2005GL022403.

Mees, J., S. Crewell, H. Nett, G. Delange, H. Vandestadt, J. J. Kuipers, and R. A. Panhuyzen (1995), Asur—An airborne sis receiver for atmospheric measurements of trace gases at 625 to 760 ghz, *IEEE Trans. Microwave Theory Tech.*, *43*(11), 2543–2548.

Neu, J. L., L. C. Sparling, and R. A. Plumb (2003), Variability of the subtropical "edges" in the stratosphere, *J. Geophys. Res.*, *108*(D15), 4482, doi:10.1029/2002JD002706.

Pierrehumbert, R. T. (1994), Tracer microstructure in the large-eddy dominated regime, *Chaos Solitons Fractals*, *4*(6), 1091–1110.

Pierrehumbert, R. T. (2000), Lattice models of advection-diffusion, *Chaos*, *10*(1), 61–74.

Press, W., S. Teukolsky, W. Vetterling, and B. Flannery (1992), *Numerical Recipes in FORTRAN—The Art of Scientific Computing*, 2nd ed., Cambridge Univ. Press, New York.

Proffitt, M., et al. (1989), In situ ozone measurements within the 1987 Antarctic ozone hole from a high-altitude ER-2 aircraft, *J. Geophys. Res.*, *94*(D14), 16,547–16,555.

Rood, R. B., A. R. Douglass, M. C. Cerniglia, L. C. Sparling, and J. E. Nielsen (2000), Seasonal variability of middle-latitude ozone in the lowermost stratosphere derived from probability distribution functions, *J. Geophys. Res.*, *105*(D14), 17,793–17,805.

Russell, J. M., et al. (1993), The Halogen Occultation Experiment, *J. Geophys. Res.*, *98*(D6), 10,777–10,797.

Russell, J. M., et al. (1996), Validation of hydrogen chloride measurements made by the Halogen Occultation Experiment from the UARS platform, *J. Geophys. Res.*, *101*(D6), 10,151–10,162.

Schoeberl, M. R., et al. (1989), Reconstruction of the constituent distribution and trends in the Antarctic polar vortex from ER-2 flight observations, *J. Geophys. Res.*, *94*(D14), 16,815–16,845.

Schoeberl, M. R., L. C. Sparling, C. H. Jackman, and E. L. Fleming (2000), A Lagrangian view of stratospheric trace gas distributions, *J. Geophys. Res.*, *105*(D1), 1537–1552.

Sparling, L. C. (2000), Statistical perspectives on stratospheric transport, *Rev. Geophys.*, *38*(3), 417–436.

Sparling, L. C., and M. R. Schoeberl (1995), Mixing entropy analysis of dispersal of aircraft emissions in the lower stratosphere, *J. Geophys. Res.*, *100*(D8), 16,805–16,812.

Strahan, S. (2002), Influence of planetary wave transport on Arctic ozone as observed by Polar Ozone and Aerosol Measurement (POAM) III, *J. Geophys. Res.*, *107*(D20), 4417, doi:10.1029/2002JD002189.

Toon, G. C., et al. (1999), Comparison of MKIV balloon and ER-2 aircraft measurements of atmospheric trace gases, *J. Geophys. Res.*, *104*(D21), 26,779–26,790.

Waters, J. W., et al. (2006), The Earth Observing System Microwave Limb Sounder (EOS MLS) on the Aura satellite, *IEEE Trans. Geosci. Remote Sens.*, *44*(5), 1075–1092.

Yang, H. J. (1995), 3-dimensional transport of the ertel potential vorticity and N_2O in the GFDL skyhi model, *J. Atmos. Sol. Terr. Phys.*, *52*(9), 1513–1528.

Zander, R., M. R. Gunson, C. B. Farmer, C. P. Rinsland, F. W. Irion, and E. Mahieu (1992), The 1985 chlorine and fluorine inventories in the stratosphere based on ATMOS observations at 30-degrees north latitude, *J. Atmos. Chem.*, *15*(2), 171–186.

————————————

O. Aulov and D. J. Lary, Goddard Earth Sciences and Technology Center, University of Maryland Baltimore County, Baltimore, MD 21228, USA. (david.lary@umbc.edu)